NANO LETTERS

Letter

pubs.acs.org/NanoLett

Interface-Induced Nucleation, Orientational Alignment and Symmetry Transformations in Nanocube Superlattices

Joshua J. Choi,[†] Kaifu Bian,[‡] William J. Baumgardner,[§] Detlef-M. Smilgies,[∥] and Tobias Hanrath[‡,*]

[†]School of Applied and Engineering Physics, [‡]School of Chemical and Biomolecular Engineering, [§]Department of Chemistry and Chemical Biology, and [∥]Cornell High Energy Synchrotron Source, Cornell University, Ithaca, New York 14853, United States

Supporting Information

ABSTRACT: The self-assembly of colloidal nanocrystals into ordered superstructures depends critically on the shape of the nanocrystal building blocks. We investigated the self-assembly of cubic PbSe nanocrystals from colloidal suspensions in real-time using *in situ* synchrotron-based X-ray scattering. We combined small-angle and wide-angle scattering to investigate the translational ordering of nanocrystals and their orientational ordering in the lattice sites, respectively. We found that cubic PbSe nanocrystals assembled into a face-up (i.e., ⟨100⟩ normal to the interface) configuration at the liquid/substrate interface whereas nanocubes at the liquid/air interface assume a corner-up (i.e., ⟨111⟩ normal to the interface) configuration. The latter nanocrystal superlattice displays polymorphism as a function inter-NC separation distance. We explain the observed superlattice structure polymorphs in terms of the interactions directing the self-assembly. Insights into the directed self-assembly of superlattices gained from this study have important implication on the future development of nanocrystals as building blocks in artificial solids.

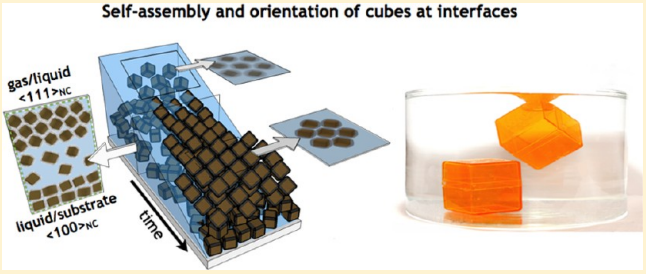

KEYWORDS: *Nanocrystals, superlattice, self-assembly, in situ X-ray scattering, interface effects*

Access to colloidal nanocrystals (NCs) with well-defined size and shape has created intriguing opportunities for scientists and engineers to assemble ordered superstructures with properties by design. As a result of intensive research efforts, the concept of NC assemblies as an artificial solid comprised of NCs as artificial atoms has rapidly evolved from an academic curiosity toward a versatile test ground to experimentally probe emerging properties in coupled quantum confined systems and development of related technologies.[1,2] The novel structural, optical, electronic, and magnetic properties[2−5] that are predicted to emerge as a result of collective interactions between NCs in the assembly have inspired the quest for better understanding and controlling the self-assembly of superstructures from colloidal suspensions.

Cubic nanocrystals (cNCs) in particular have been subject of increasing research efforts for several reasons. From an electronic perspective, cNCs provide a convenient basis for theoretical studies of the emerging electronic structure in coupled semiconductor quantum dot arrays.[4] The shape of the building block significantly influences interparticle coupling.[6−9] For example, effective mass quantum mechanical calculations of 2-dimensional NC assemblies have shown that the coupling energy between face-to-face oriented cubes is three times larger than between spheres.[10] These electronic effects are particularly pronounced in strongly quantum confined systems, the most prominent example of which are lead salt (PbX; X = S, Se, and Te) NCs. The unique electronic properties of PbX NCs have been underscored by recent reports of successful prototype photovoltaics,[11,12] including harvesting of multiexcitons,[13,14] light-emitting diodes,[15] electronics[16,17] and thermoelectrics.[18,19] Koh et al. recently demonstrated the strong coupling between the cNCs to create high mobility and high gain CMOS-like inverters.[17] Most of the prototype devices reported to date involve disordered NC thin films. Yet, to fully harness the scientific and technological opportunities of NC assemblies as tunable artificial solids with electronic structure by design, detailed control and understanding of the self-assembly into ordered and functional superstructures are desirable.

Compared to spherical particles, which generally assemble in close-packed structures, nonspherical particles exhibit a much larger diversity of superstructures.[6,20−26] Moreover, the anisotropic interactions governing the self-assembly also lead to orientational ordering of neighboring particles in the assembly and in some cases a direct connection between orientational alignment and superlattice symmetry has been found.[22] However, the self-assembly of the superstructure is not solely governed by geometric considerations of the shape of the building blocks; a complex interplay of van der Waals, electrostatic, magnetic, molecular, and entropic effects needs to be considered.[20] Monte Carlo simulations have predicted cubic particles to exhibit a rich phase diagram of superstructures ranging from isotropic structures (at low packing fraction) to

Received: June 12, 2012
Revised: August 9, 2012
Published: August 13, 2012

   dx.doi.org/10.1021/nl3026289 | *Nano Lett.* 2012, 12, 4791−4798

cubatic mesophases to close packed structures with unity packing fraction.[27] Experimental studies of colloidal cNCs, by Gang and co-workers, revealed the phase transition behavior of the superlattice structure between simple cubic and rhombohedral phases depending on the ligand shell thickness.[25] More recently, Petit and co-workers reported the relationship between the detailed shape of the cNC (i.e., truncated and regular cubes) and the structure of the superlattice.[28]

Apart from the interactions between particles, it is also critical to understand the interaction between the particles and macroscopic interfaces, between the suspension and both the vapor phase above as well as the solid substrate below;[29−31] these effects are particularly pronounced in the self-assembly of thin films from colloidal cNC suspensions.[32,33] The nature of the interactions between the particles and the interface is fundamentally different from the interactions among particles in the bulk. The role of these interface effects in the self-assembly of superstructures from anisotropic particles is not well understood and is the focus of this letter. We report *in situ* X-ray scattering measurements to probe the emergence of translational and orientational order during the self-assembly of the superlattice from suspended cNCs. Remarkably, we discovered that cNC assemble in two different configurations, namely "face-up" (i.e., ⟨100⟩ normal to the interface) at the liquid/substrate interface and "corner-up" (i.e., ⟨111⟩ normal to the interface) at the gas/liquid interface. These results provide important new insights into the fundamental interactions governing self-assembly of superlattices from colloidal suspensions and underscore the vital role of interface effects.

Results and Discussion. PbSe cNCs can serve as a model system for a variety of reasons. First of all, cNC with uniform size and shape can be reliably prepared by established hot-injection synthesis methods.[34] Second, lead salt NCs present one of the most strongly quantum confined systems, with the effect that the electronic structure of lead salt NCs with dimensions in the range of 10−15 nm are still considerably impacted by quantum confinement[35] and thus provide intriguing opportunities for scientific studies of artificial solids as well as novel device applications. Figure 1 shows low- and high-resolution transmission electron microscopy (TEM) images of the PbSe cNC building blocks used in this study. Statistical analysis of TEM images revealed an average edge length of 13.3 nm with a relative polydispersity of 8.2% (Figure 1b). The narrow size distribution in the cNC synthesis was enabled by advances in the colloidal synthesis of cubes;[36] in our case the refined size control was achieved through a better understanding of the relationship between the time−temperature profile of the synthesis and the particle shape.[37] High-resolution TEM images reveal deviations in the particle shape between the colloidal cNC (Figure 1d) and the idealized model (Figure 1c), notably, the atomically resolved TEM image shows that the edges of the cNC are not sharp, but instead appear to be rounded by {110} facets.

To form a self-assembled thin film of the cNCs, we drop-cast a suspension of the particles in hexane (5 mg mL^{-1}) onto a cleaned silicon wafer and allowed the solvent to slowly evaporate (over 8 h) in a nearly saturated solvent vapor environment (see Supporting Information for details). We analyzed the structure of the self-assembled cNC thin films using grazing-incidence small-angle X-ray scattering (GISAXS) and grazing-incidence wide-angle X-ray scattering (GIWAXS) on the same sample position. The combination of wide- and small-angle X-ray scattering is particularly powerful for the

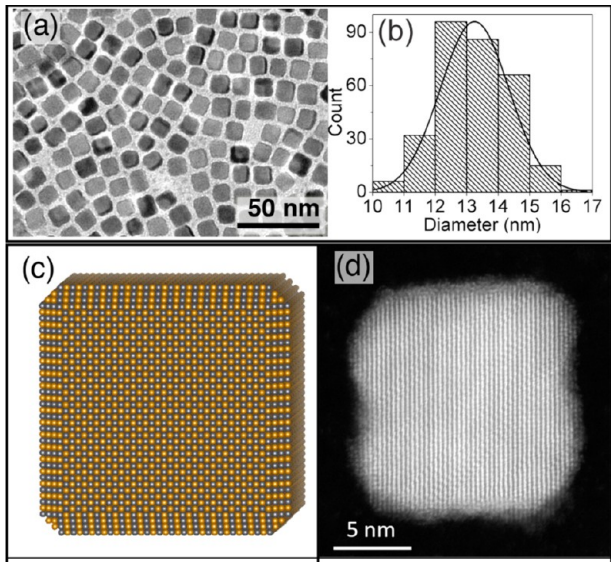

Figure 1. cNC building blocks. Key: (a) low-resolution TEM image of the PbSe cNCs; (b) histogram of cNCs edge length; (c) model structure of an ideal PbSe cNC showing six {100} facets and small area {110} facets along the edge of the cube; (d) high-resolution TEM image showing detailed atomic structure of PbSe cNC.

structural characterization of NC superlattices: GISAXS reveals the translational ordering of the particles, whereas GIWAXS provides information about the orientational ordering of NCs in their superlattice sites.[22,33,38] Analysis and indexing of the information-rich scattering patterns provides detailed insights into the superlattice structure including the interparticle spacing, possible lattice distortions, and average grain size. To delineate between the crystallographic planes of the nanocrystal and the superlattice we will denote scattering planes and directions with subscripts "NC" and "SL", respectively.

Figure 2 shows the GISAXS pattern of a PbSe cNC superlattice which can be uniquely indexed as rhombohedral (RH) structure with $\{111\}_{SL}$ planes parallel to the substrate, lattice constant, a = 16.2 nm and angle, α = 68.8°. The dry self-assembled cNC films had a typical thickness of 50 nm as determined by cross-sectional SEM image analysis (see Supporting Information) corresponding to three to four layers of nanocubes. RH superlattices have been reported in literature before: Dunphy et al. found RH-distorted layers in deposits of spherical gold particles.[39] In this case capillary forces during drying distorted the FCC lattice. More recently Gang and co-workers reported RH structures in cNC with rounded edges from which they found that the amount of the RH distortion could be correlated with the degree of rounding of the corners.[25] Sharp corners result in RH structures close to SC ordering whereas rounded corners induce RH structures close to FCC, which is the stable limit for hard spheres. By simple geometric arguments one would have expected the SC lattice to be the stable lattice for cNCs, however, experimental reports on simple cubic superlattices of cNCs have been scarce. Brückel and co-workers recently reported a tetragonal packing of iron oxide cNCs where second layer cNC sit in the 4-fold hollow between the four adjacent cNC of the layer below, and the vertical distance between adjacent layers was considerably smaller than would be expected for the packing of hard cubes.[40] This result shows that ligand−ligand interactions between cNC

dx.doi.org/10.1021/nl3026289 | *Nano Lett.* 2012, 12, 4791−4798

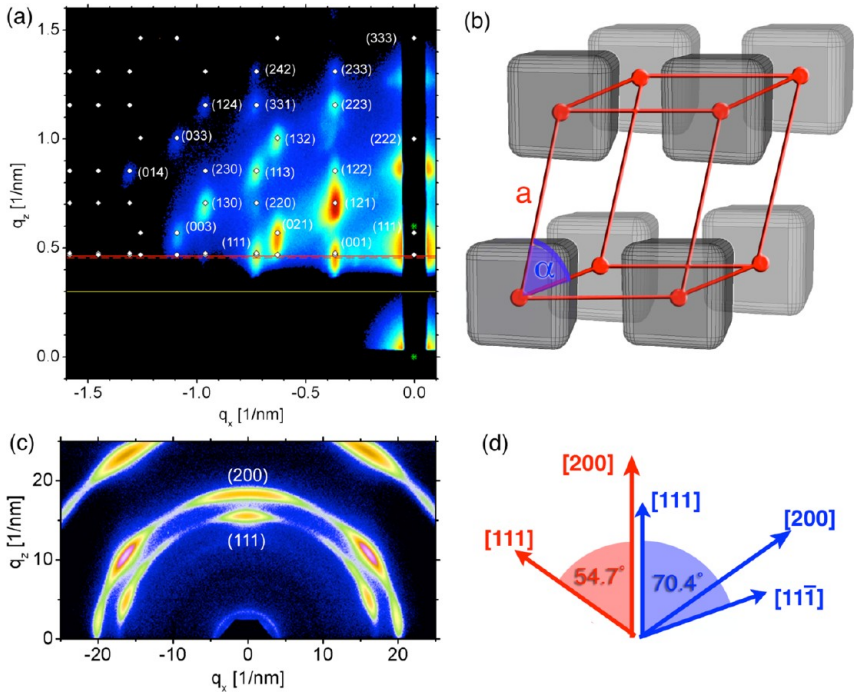

Figure 2. Structure of PbSe cNC superlattices. Key: (a) GISAXS pattern of a PbSe cNC superlattice indexed to RH structure with $(111)_{SL}$ planes parallel to the substrate; (b) model of RH superlattice structure with lattice constant, a, and lattice angle, α; (c) GIWAXS pattern shows coexistence of two types of NC orientations—one orientation where $(100)_{NC}$ planes are parallel to the substrate (lying face-down on the substrate) and the other orientation where $(111)_{NC}$ planes are parallel to the substrate (NCs are pointing the corner toward the substrate); (d) schematic illustration of the relationship between $\{111\}_{NC}$ and $\{200\}_{NC}$ reflections for face-up (red) and corner-up (blue) oriented cNC.

in adjacent layers is complex and that "soft cubes" can feature a surprising variety of structures.

The nearest-neighbor separation in the RH structure is between $\{100\}_{NC}$ facets of proximate cNC. We determine the surface-to-surface distance as $\delta = \xi_{(\alpha)}a - d_{NC}$ where a is the superlattice constant (a = 16.2 nm, measured by GISAXS), $\xi_{(\alpha)}$ is a geometric factor accounting for the lattice angle α (see Supporting Information Figure S6 for details) and d_{NC} is the average cNC edge length (d_{NC} = 13.3 nm, determined from TEM image analysis). For the lattice parameters given above, we determine δ = 2.1 nm, which is smaller than twice the length of oleic acid molecules (1.8 nm). This suggests that the ligands bound to adjacent parallel $\{100\}_{NC}$ facets are either interdigitated or are tilted on the faces of the cNCs, which is consistent with our earlier studies of assemblies of cuboctahedra shaped PbSe NCs.[22,38] The volume fraction of the inorganic cNC cores in the superlattice is 0.66, which compares well with the packing fraction (0.6) observed in our earlier measurements with cuboctahedra PbS NC.[22]

The RH structure shown in Figure 2b is equivalent to a face-centered cubic (FCC) structure with a 18% lattice contraction in the $\langle 111\rangle_{SL}$ direction, *i.e.* perpendicular to the substrate plane. RH, FCC, and simple cubic (SC) structures can be related through a continuous phase transformation path from FCC (α_{FCC} = 60°) to SC (α_{SC} = 90°)[25,41,42] via RH structures with intermediate angles (60° < α_{RH} < 90°). The FCC-to-SC transformation has been observed in a variety of atomic lattices and recently also in NC superlattices.[25,41,42] We note that the lattice shrinkage along $\langle 111\rangle_{SL}$ can also arise from drying stresses imposed by capillary forces similar to prior observations in nanoparticle and polymer thin films.[33,39,43,44] We have previously shown that superlattices formed from lead salt cuboctahedra NCs also exhibit superlattice constant shrinkage perpendicular to the plane of the substrate, although the lattice distortion (~5%) in FCC superlattices of cuboctahedra NC is significantly smaller than the 18% observed for the RH assembly of cNC.[33] Gang et al. have recently attributed the RH lattice distortion to the shape of the nanocube, i.e., rounding of the corners of the cube.[25]

To understand the role of the cNC shape in the assembly of the RH superlattice, we probed the orientational ordering of cNCs in their superlattice sites using GIWAXS. The wide-angle scattering pattern in Figure 2c is intriguing because the $\{111\}_{NC}$ and $\{200\}_{NC}$ peaks both reflect normal to the plane of the substrate (at a detector azimuth of 0°) which suggests that there are two mutually exclusive orientations of cNCs within the film. This scattering pattern indicates that a fraction of cNCs show an orientation of $\langle 111\rangle_{NC}$ normal to the substrate (i.e., a "corner-up" configuration), while other cNCs exhibit $\langle 100\rangle_{NC}$ normal to the substrate (i.e., a "face-up" configuration). Figure 2d schematically illustrates the relationship between reflections from $\{111\}_{NC}$ and $\{200\}_{NC}$ as a function of azimuthal angle for both face-up (red) and corner-up (blue) oriented cNC.

The peculiar superlattice structure and orientation revealed by the small-angle and wide-angle scattering patterns raise several questions. (i) How can cNCs assemble into an ordered superlattice structure in which the cubes have two orientations: "face-up" and "corner-up"? Do these orientations reflect homogeneously and heterogeneously nucleated structures or do they arise from interactions with the macroscopic interfaces? (ii) Do the observed superlattice symmetries represent equilibrium structures or do they reflect liquid-crystal like mesophase structures that are kinetically trapped during the solvent evaporation? (iii) Does the distorted superlattice structure reflect the inherent symmetry of the cNC assembly

dx.doi.org/10.1021/nl3026289 | *Nano Lett.* 2012, 12, 4791−4798

or does this structure arise due to shrinkage during solvent evaporation? To answer these questions and to differentiate between alternate hypotheses we studied the superlattice formation under carefully selected experimental conditions.

Superlattices formed by homogeneous nucleation can be easily differentiated from structures heterogeneously nucleated at thin film interfaces on the basis of the superlattice orientation relative to the substrate. We previously showed that rapid supersaturation leads to homogeneous nucleation of superlattice grains that precipitate in random orientation relative to the substrate.[33] Such a scenario would have resulted in Debye–Scherrer rings in the GISAXS pattern[33] and powder-like rings in GIWAXS. In light of the observed preferential ordering relative to the substrate for both SL and NC orientation evidenced by the small- and wide-angle scattering, we conclude that the self-assembled structures were nucleated heterogeneously at interfaces and not homogeneously within the bulk suspension.

Next, we discuss a series of experiments devised to better understand the role of the gas/liquid and liquid/solid interface in the heterogeneous superlattice nucleation. Monolayer cNC films present an advantageous experimental system to investigate the interface effects. We formed monolayer superlattices from dilute suspensions (0.5 mg mL^{-1}) under controlled evaporation conditions. The GISAXS pattern (Figure 3a) of the superlattice formed from the dilute suspension is consistent with the scattering signature of a cNC monolayer of "face-up" oriented cubes.[45] The orientational ordering revealed by GIWAXS (Figure 3b) shows almost exclusively $\langle 100 \rangle_{NC}$ face-up orientation normal to the substrate, consistent with GISAXS. Assemblies of cNC oriented with their $\{100\}_{NC}$ facets facing the substrate have been reported in several previous cases and have been attributed to strong van der Waals interaction between the flat cube facet and the substrate.[29,30]

The translational order in the monolayer can be indexed as a 2D cubic lattice; the oscillation of the intensity along the scattering rods can be attributed to the cNC form factor.[45] Contrary to the scattering from a monolayer of spherical particles,[45] we found that the in-plane spots broadened at higher scattering vectors. This effect can by ascribed to disorder of the second type, as described within the paracrystal model.[46] In either case the intensity of higher-order reflections is suppressed, however, in disorder of the first type the peak width is not affected.[45] Interestingly, a similar finding has previously been reported in colloidal crystals studied by Dullens and Petukhov[47] who found that spherical and nonspherical colloids featured similar differences in behavior. SEM images (Figure 3c) confirm the complex structure of the cNC monolayer; however, Fourier transform image analysis was inconclusive and suggests both hexagonal and square translational ordering. We note that the structure of cNC monolayers did not depend on solvent evaporation rate, since similar structures were obtained in slow (8 h) and fast (~ 1 min) dried films.

To differentiate between kinetically trapped mesophases and equilibrium structures, we investigated the dynamics and intermediate states during the superlattice self-assembly using an *in situ* X-ray scattering chamber.[22] Importantly, this chamber enables X-ray structure characterization of self-assembled superlattices in real time and in dynamically controlled solvent vapor environments. To study the self-assembly of the cNCs *in situ*, a suspension of the particles in hexane (5 mg mL^{-1}) was drop-cast on a cleaned silicon wafer and the suspension drop

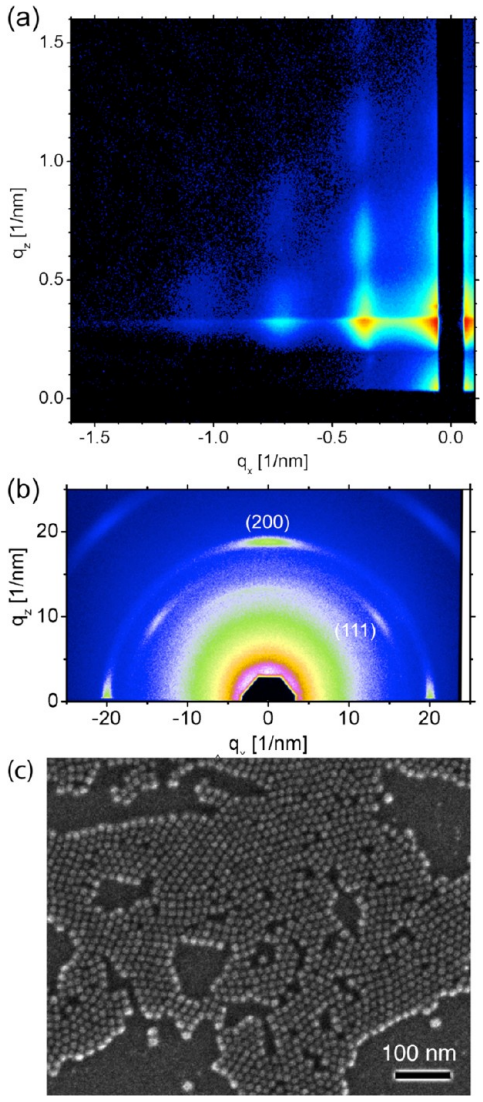

Figure 3. cNC monolayers formed from dilute colloidal suspensions. (a) The GISAXS pattern is consistent with a square monolayer of cubes. (b) GIWAXS illustrates the preferred face-up ($\langle 100 \rangle_{NC}$) orientation of cNC in the monolayer. (c) SEM image illustrates the structure of the monolayer.

was allowed to equilibrate with controlled hexane vapor concentration environment. After the equilibrium had been reached, GISAXS and GIWAXS patterns from the same sample spot were obtained.

The evolution of the translational order in the drying superlattice is summarized in Figure 4a (corresponding GISAXS patterns are provided in the Supporting Information). The scattering of the superlattice nucleated in the nearly saturated solvent environment can be uniquely indexed to a RH structure with a lattice constant, a = 18.8 nm and angle, α = 62.5°. Considering the 13.3 nm edge length of the cNC, the freshly nucleated superlattice is characterized by a surface-to-surface spacing of 4.6 nm, which is substantially larger than the twice the length of the oleic acid ligand. The structure analysis suggests that surface bound oleic acid ligands do not directly interact in the initial superlattice nucleus and that the interstitial volume of the nucleated structure contains a significant fraction of solvent (hexane). Analysis of the early stage superlattice structure provides important clues to understand the

dx.doi.org/10.1021/nl3026289 | *Nano Lett.* 2012, 12, 4791–4798

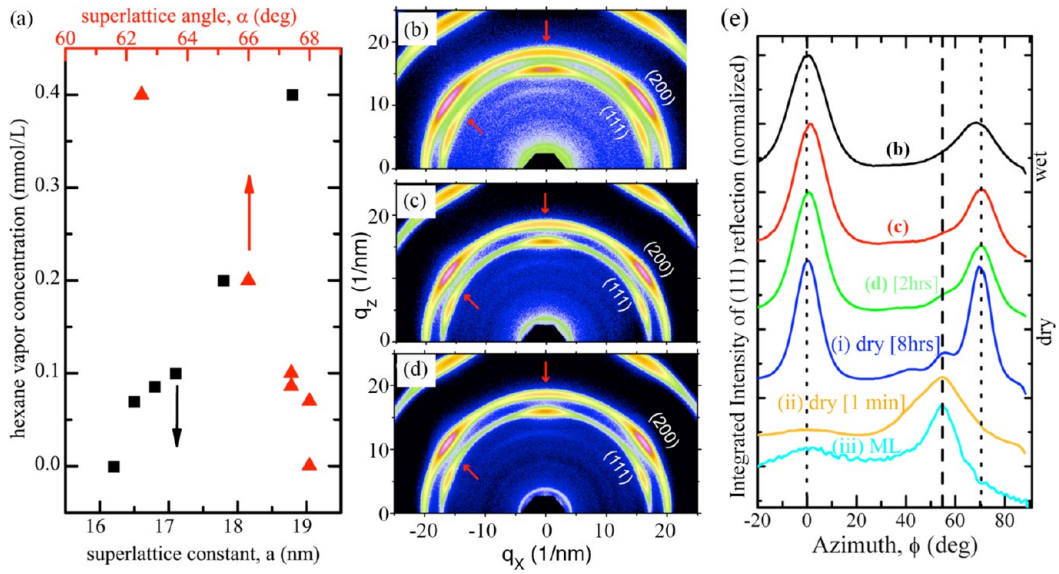

Figure 4. *In situ* X-ray scattering signatures of superlattice formation. (a) Small-angle scattering reveals the evolution of the RH superlattice constant, *a*, and angle, α as a function of hexane vapor concentration from wet (nearly saturated) to dry (pure He gas environment). Wide-angle scattering patterns (b–d) show the evolution of the orientational ordering from the wet film to the dry superlattice. (e) Radially integrated intensity of the $\{111\}_{NC}$ reflection illustrates the preferential cNC orientation in the wet and dry films (b–d) as well as assemblies formed by slow (i) and fast (ii) evaporation. The monolayer film (iii) also illustrates preferential "face-up" alignment of the cNC.

mechanism and the preferred $\langle 111\rangle_{NC}$ orientation. Since the spacing between cNC surfaces in the nascent superlattice (δ = 4.6 nm) exceeds the reach of the ligands (length of oleic acid ~1.8 nm), interactions between the particles appear to be modulated through a diffuse ligand and solvent shell surrounding the particles.

The packing fraction of the inorganic cNC core in the nascent superlattice is approximately 0.47. Interestingly, this packing fraction is within experimental error of the theoretically predicted onset of the cubatic phases (0.52);[27] however, in contrast to theoretical prediction, our experiments suggest that the nascent superstructure exhibits both orientational and translational order. We note that with our current experimental setup the transition from between small and wide angle scattering measurements takes approximately one minute; further experiments are required to probe the existence of transient liquid-crystal like cubatic phases.

Dynamic control over the hexane vapor concentration in the sample chamber allowed us to directly monitor the evolution of the superlattice structure in the drying film. We gradually reduced the hexane vapor concentration in the *in situ* chamber from saturated hexane (~ 8 mmol/L) to an almost dry helium environment over the course of two hours. For each scattering measurement, the cNC suspension was allowed to reach equilibrium with the adjusted hexane vapor concentration. Figure 4a shows that the superlattice constant, *a*, shrinks from 18.8 to 16.5 nm while the lattice angle, α, increases from 62.5° to 68° as the film dries. The fact that the lattice distortion was observed in a wet film in equilibrium with the saturated vapor environment suggests that the distortion is not due to the drying stress[33,39,43,44] but instead appears to arise from a change in the nature of the interaction between cNC as they come closer together in the drying film (*vide infra*).

The *in situ* GIWAXS patterns in Figure 4b–d illustrate how cNC orientation evolves from the "wet" to the "dry" film. We probed the nucleation of the superlattice by carefully monitoring the first distinct scattering features from "wet" film at equilibrium with nearly saturated hexane vapor concentration. Strikingly, the scattering patterns show exclusively preferential $\langle 111\rangle_{NC}$ orientation normal to the plane of the film. Specifically, the $\{111\}_{NC}$ reflections in Figure 4b are only observed at azimuth angles of 0° and 70.4°; whereas $\{200\}_{NC}$ reflections only occur at 54.7°. This scattering signature is consistent with a pure corner-up (i.e., $\langle 111\rangle_{NC}$) orientation of the cNC (see Figure 2d). As the hexane vapor concentration is reduced, $\{200\}_{NC}$ reflections started to appear at 0°, suggesting that a fraction of the cNC have oriented in the "face-up" (i.e., $\langle 100\rangle_{NC}$) configuration (Figure 4c,d). To more clearly illustrate the evolution of the orientational ordering we show the integrated intensity of the $\{111\}_{NC}$ reflection rings as a function of azimuthal angle (Figure 4e). The integrated $\{111\}_{NC}$ ring shows the emergence of increased scattering at an azimuth of 54.7° as the film evolves from wet to dry, indicating that more cNCs form the face-up orientation.

As a way to investigate how the orientational alignment relates to the dynamics of the self-assembly from the colloidal suspension, we formed cNC superlattice at various drying rates. We observed the most pronounced signature of "corner-up" oriented cNC from assemblies formed with a 2-h drying time (Figure 4c). Films formed with slower drying times (eight hours), showed weaker contribution from 'corner-up' particles (Figure 2b and (i) in Figure 4e). Superlattice films formed by rapid solvent evaporation in ambient environment show exclusively 'face-up' orientation ((ii) in Figure 4d) (scattering patterns and structural analysis of the rapidly dried cNC films are provided in the Supporting Information, Figure S5). This trend illustrates the complex relationship between the dynamics and the structure of the self-assembled film, which we explain in the model introduced below. For reference, Figure 4e also includes the integrated intensities of the GIWAXS pattern of the cNC monolayer (Figure 3) to show the dominant peak $\{111\}_{NC}$ reflection at an azimuth of 54.7°, consistent with the preferential "face-up" ordering in the cNC monolayer.

dx.doi.org/10.1021/nl3026289 | *Nano Lett.* 2012, 12, 4791–4798

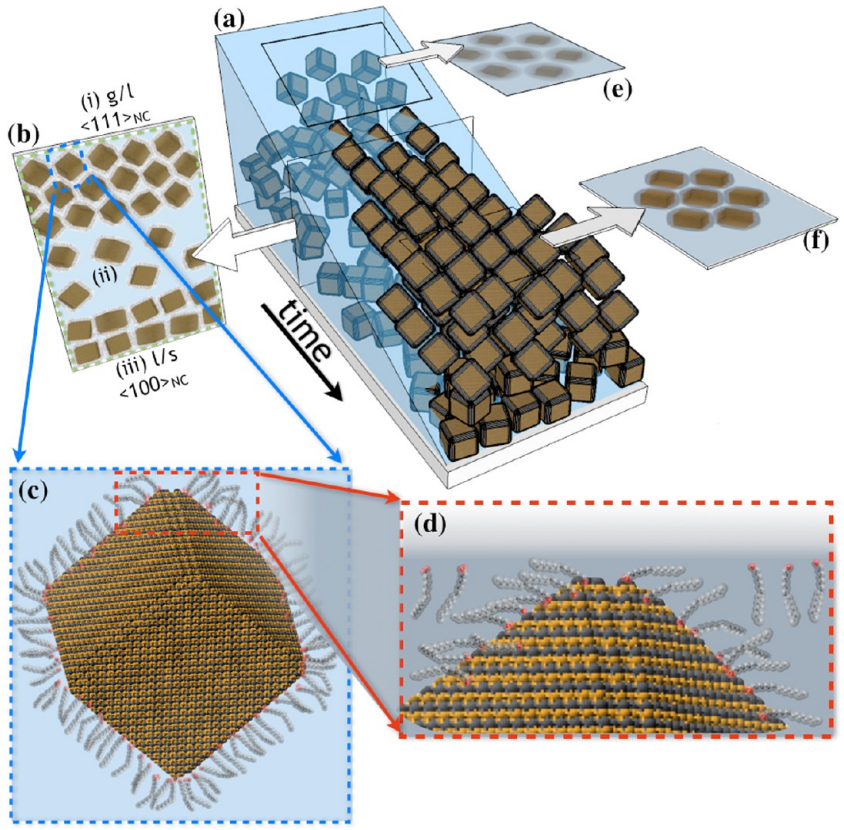

Figure 5. Schematic illustration of the proposed mechanism for cNC superlattice formation. (a) Schematic of the temporal and spatial evolution of self-assembled cNC superstructures. (b) Slice at intermediate drying times illustrating three key regions: (i) gas/liquid interface, (ii) the bulk liquid suspension, and (iii) the liquid/solid interface. The thickness of the liquid suspension decreases from left to right as the solvent evaporates. (c) Magnified view of the cNC near the gas/liquid interface and (d) the structure of the ligand near the interface. The insets (e, f) illustrate the formation of the hexagonal two-dimensional seed layer and the resulting orientational alignment of cNC.

Insights from the scattering data detailed above allow us to propose the following mechanism to describe the superlattice nucleation, the coexistence of two distinct cNC orientations, and the relationship between the dynamics of the self-assembly and the resulting structure. Importantly, the structure of the observed RH cNC superstructures appears to be induced by interactions between the particles and the macroscopic interfaces. Figure 5 schematically illustrates the temporal and spatial (i.e., vertical) variation in cNC orientation and structure of the emerging superlattice. We first consider the spatial variations illustrated by the cross-sectional slice taken at an intermediate drying time (Figure 5b). Three regions in the film are delineated by their vertical position and their proximity to macroscopic interfaces, namely: (i) the interface between the colloidal suspension and the gas above, (ii) the bulk liquid suspension, and (iii) the interface between the suspension and the solid substrate. It is important to recognize that the particle concentration varies as a function of height; this is not a gravitational effect, but rather a consequence of the interfacial interactions between the colloidal suspension and both gas and solid interface (region i and iii in Figure 5b respectively). The magnitude of the vertical cNC concentration gradient depends on the overall concentration and the relative surface energies at both interfaces.

Molecular surfactants and colloidal particles alike tend to adsorb at interfaces since the adsorption lowers the free energy of the system.[48] The formation of a Gibbs monolayer near the gas/liquid interface is one manifestation of this effect, which can be directly measured by the reduction of the surface tension of the solution.[49,50] Campolongo et al. have recently explored Gibbs monolayer formation with DNA-capped nanoparticles at the interface.[51] At particle concentrations below the supersaturation limit, NCs in the bulk liquid sufficiently far from the interface (*i.e.*: region ii in Figure 5) are homogenously distributed in the suspension. We note that cNC in the subsaturated suspension can occur as a mixture of monomers (i.e., isolated particles) and short oligomers (i.e., chains of up to approximately 5−6 particles), as illustrated in a recent study by Rijssel et al.[52] In analogy to the formation of atomic and molecular crystals, the supersaturation provides the driving force for the superlattice formation, whereas the creation of the interface between the superlattice and the surrounding environment presents an energetic penalty. Superlattice nucleation at the interface is thus favored over nucleation in the bulk due to two factors: first, the concentration near the interface is larger as discussed above and second the free energy change for heterogeneous nucleation is less than for homogeneous nucleation.

The cross-sectional slice in Figure 5b illustrates that the preferred orientation of cNC at the gas/liquid interface (region *i*) is corner up or $\langle 111 \rangle_{NC}$ whereas particles at liquid/solid interface (region *iii*) assume the face-up $\langle 100 \rangle_{NC}$ orientation. We propose to explain the difference in preferred orientation based on thermodynamic considerations of particle orientations and the molecular configuration of the ligand near the interface. At the liquid/solid interface, the particles deposit in the face-up

dx.doi.org/10.1021/nl3026289 | *Nano Lett.* 2012, 12, 4791−4798

$\langle 100\rangle_{NC}$ orientation; this configuration is favored the strong van der Waals interaction between the particles and the substrate.[32] At the gas/liquid interface, more complex interactions have to be considered. By itself, free oleic acid surfactants and unbound lead oleate would form a Gibbs monolayer near the gas/liquid interface. In the energetically preferred configuration, the polar carboxylic acid group would point toward the interface allowing the aliphatic tail to be well solvated in the bulk liquid phase. This molecular configuration is illustrated in Figure 5d. As ligands, oleic acid is chemically attached to the NC surface via the carboxylic acid group; this constrains the molecular configurations of the ligand. Ligands near the interface, and the cNC as a whole, will thus orient in a way to provide the most solvation for the aliphatic ligand chain. The $\langle 100\rangle_{NC}$ configuration would be unfavorable at the gas/liquid interface since it maximizes the number of ligands exposed to the vapor interface. On the other hand, the $\langle 111\rangle_{NC}$ corner-up orientation (Figure 5c) would provide the best solvation for the majority of the ligand chains and thus should present the energetically preferred configuration. The detailed structure of cNCs near the interface (*i.e.*: whether the particle is fully submerged or partially protrudes from the gas/liquid interface) is governed by a complex interplay of the particle concentration, the wettability of the cNC surface in the solvent, the presence of desorbed ligands, etc. Law and co-workers have recently reported a model of NC adsorption at the gas/liquid interface to account for line tension effects and wettability.[50] On the basis of their model and the surface energies of the hexane (solvent)/oleic acid (ligand) system at the focus of our work, we are led to conclude that the solvent completely wets the ligand shell and that the particle is fully submerged below the gas/liquid interface.

A closer look at interactions between cNCs in the plane of the monolayer seeding the superlattice growth at the gas/liquid interface further clarifies the preferred $\langle 111\rangle_{NC}$ orientation. The hexagonal translational order in the nascent seed layer (Figure 5e) naturally favors the $\langle 111\rangle_{NC}$ orientation since this configuration provides a 3-fold symmetry of the cNC and thus balances the in-plane interactions among cNCs; other cNC orientations within the seed layer would face imbalanced interactions (see Supporting Information, Figure S7). Figure 5f illustrates how the hexagonal translational structure in the monolayer re-enforces the "corner-up" orientational ordering of the cNC in their lattice sites. Importantly, this model can explain how the hexagonal ordering of $\langle 111\rangle_{NC}$ orientated cNC in the seed layer successively induces the self-assembly of RH superlattice symmetry in thicker films.

Although the thermodynamic considerations discussed above successfully capture the preferred cNC orientation near the interfaces, the observed relationship between drying rates and measured cNC orientation suggests that kinetic aspects also influence the self-assembly of the superstructure. To describe the kinetic aspects, we will first try to explain the absence of $\langle 111\rangle_{NC}$ in cNC films formed by rapid solvent evaporation. In that case, the rapid solvent evaporation prevents the formation of a Gibbs monolayer at the interface. Law and co-workers observed that it took on the order of half an hour for the surface tension of a drop of nanoparticle solution equilibrated in solvent vapor to stabilize.[50] This observation indicates that the formation of the Gibbs layer at the vapor-solvent interface is a slow diffusion-limited process. In the case of rapidly formed cNC thin films, the hexagonal seed layer could not form the gas/liquid interface and the emerging structure is dominated by $\langle 100\rangle_{NC}$ alignment induced by interactions between the particles and the substrate.

Interface-induced orientational (re)ordering can also explain the trend of preferred "corner-up" orientation at intermediate drying times compared to the coexistence of "corner-up" and "face-up" orientations in the slowly dried film. The interface between the $\{111\}_{SL}$ superlattice planes with $\langle 111\rangle_{NC}$ orientation nucleated at the gas/liquid interface and cubic superlattice with $\langle 100\rangle_{NC}$ orientation formed at the solid substrate represents a frustrated system. We can therefore understand the enhanced $\langle 100\rangle_{NC}$ orientation in the slowly dried film as a result of reordering of cNC at the interface between region i and iii. In other words, slow drying times appear to facilitate a substrate-induced "corner-up"-to-"face-up" transformation.

The dynamics of monolayer formation at the gas/liquid interface and orientational reordering at the solid/solid interface (between region i and iii) are remarkable, and highlight the importance of interfacial effects in superlattice formation. Specifically, competing superlattice structures nucleating at the substrate-solution and solution−air interfaces can prevent the formation of a homogeneous superlattice film. Fortuitously, our results indicate that there seem to be kinetic pathways to favor one orientation over the other and thus achieve homogeneous superlattice structures.

Conclusion. We studied the self-assembly of colloidal cNC into ordered superstructures in real time using *in situ* X−ray scattering. Dynamic control over the solvent vapor environment allowed us to directly monitor the evolution of the superlattice structure from the nascent FCC to the dried RH superlattice symmetry. We discovered that the cNC exhibit two distinct orientations, namely "face-up" and "corner-up". The coexistence of two particle orientations can be explained in terms of underlying thermodynamic and kinetic effects. The thermodynamic effect illustrates that "corner-up" oriented cNC at the vapor−solution interface can minimize their free energy by orienting themselves to maximize the contact of the ligand shell with the surrounding solvent. The kinetic effect relates the particle orientation to the formation of a hexagonally ordered Gibbs monolayer, which then locks in the orientation of the cNC in the three-dimensional superlattice. Understanding and directing the self-assembly of anisotropic NCs into ordered and functional superstructures is vital for the future scientific and technological progress of nanomaterials. The insights gained from this study provide important guidance for the role of interfaces and fundamental kinetic and thermodynamic factors governing the self-assembly of superstructures based on cNC building blocks.

■ ASSOCIATED CONTENT

Ⓢ Supporting Information

Experimental details concerning the cNC synthesis and superlattice formation, X-ray, TEM, and SEM structure characterization, in situ GISAXS at variable solvent vapor concentrations, nearest neighbor separation between $\{100\}_{NC}$ facets in the RH superlattice, and orientational ordering of cNC in the hexagonal monolayer seeding superlattice growth. This material is available free of charge via the Internet at http://pubs.acs.org.

■ AUTHOR INFORMATION

Corresponding Author

*E-mail: th358@cornell.edu.

Notes

The authors declare no competing financial interest.

■ ACKNOWLEDGMENTS

We thank Don Koch, Fernando Escobedo, Paul Steen, Terry Bigionie, and Sol Gruner for stimulating discussions. We thank Lena Kourkoutis-Fitting for assistance with the high-resolution TEM microscopy. J.J.C. was supported by the NSF IGERT Fellowship Program on "Nanoscale Control of Surfaces and Interfaces," administered by Cornell's MRSEC. K.B. was supported by NSF-DMR-1056943. W.B. was supported by the KAUST-CU Center for Energy and Sustainability. GISAXS measurements were conducted at the Cornell High Energy Synchrotron Source (CHESS), which is supported by the National Science Foundation and the National Institutes of Health/National Institute of General Medical Sciences under NSF award DMR-0225180. This publication is based on work supported in part by Award No. KUS-C1-018-02, made by King Abdullah University of Science and Technology (KAUST).

■ REFERENCES

(1) Talapin, D. V.; Lee, J.-S.; Kovalenko, M. V.; Shevchenko, E. V. *Chem. Rev.* **2010**, *110* (1), 389−458.
(2) Hanrath, T. *J. Vac. Sci. Technol. A: Vac., Surf., Films* **2012**, *30* (3), 030802−030802.
(3) Markovich, G.; Collier, C. P.; Henrichs, S. E.; Remacle, F. O.; Levine, R. D.; Heath, J. R. *Acc. Chem. Res.* **1999**, *32* (5), 415−423.
(4) Lazarenkova, O.; Balandin, A. *J. Appl. Phys.* **2001**, *89* (10), 5509−5515.
(5) Remacle, F.; Levine, R. *ChemPhysChem* **2001**, *2* (1), 20−36.
(6) Quan, Z.; Fang, J. *Nano Today* **2010**, *5* (5), 390−411.
(7) Polarz, S. *Adv. Funct. Mater.* **2011**, *21*, 3214−3230.
(8) Lapointe, C. P.; Mason, T. G.; Smalyukh, I. I. *Science* **2009**, *326* (5956), 1083−1086.
(9) Nguyen, T. D.; Jankowski, E.; Glotzer, S. C. *ACS Nano* **2011**, *5*, 8892−8903.
(10) Liljeroth, P.; Overgaag, K.; Urbieta, A.; Grandidier, B.; Hickey, S. G.; Vanmaekelbergh, D. *Phys. Rev. Lett.* **2006**, *97* (9), 096803−4.
(11) Tang, J.; Sargent, E. H. *Adv. Mater.* **2010**, *23* (1), 12−29.
(12) Kramer, I.; Sargent, E. H. *ACS Nano* **2011**, *5*, 8506−8514.
(13) Sambur, J. B.; Novet, T.; Parkinson, B. A. *Science* **2010**, *330* (6000), 63−66.
(14) Semonin, O. E.; Luther, J. M.; Choi, S.; Chen, H.-Y.; Gao, J.; Nozik, A. J.; Beard, M. C. *Science* **2011**, *334* (6062), 1530−1533.
(15) Sun, L.; Choi, J. J.; Stachinik, D.; Bartnik, A.; Hyun, B.-R.; Malliaras, G. G.; Hanrath, T.; Wise, F. *Nature Nanotechnol.* **2012**, *7*, 369−373.
(16) Chung, D. S.; Lee, J.-S.; Huang, J.; Nag, A.; Ithurria, S.; Talapin, D. V. *Nano Lett.* **2012**, *12* (4), 1813−1820.
(17) Koh, W.-k.; Saudari, S. R.; Fafarman, A. T.; Kagan, C. R.; Murray, C. B. *Nano Lett.* **2011**, *11* (11), 4764−4767.
(18) Ko, D.-K.; Murray, C. B. *ACS Nano* **2011**, *5* (6), 4810−4817.
(19) Wang, R. Y.; Feser, J. P.; Lee, J.-S.; Talapin, D. V.; Segalman, R.; Majumdar, A. *Nano Lett.* **2008**, *8* (8), 2283−2288.
(20) Bishop, K. J. M.; Wilmer, C. E.; Soh, S.; Grzybowski, B. A. *Small* **2009**, *5* (14), 1600−1630.
(21) Grzelczak, M.; Vermant, J.; Furst, E. M.; Liz-Marzan, L. M. *ACS Nano* **2010**, *4* (7), 3591−3605.
(22) Bian, K.; Choi, J. J.; Kaushik, A.; Clancy, P.; Smilgies, D.-M.; Hanrath, T. *ACS Nano* **2011**, *5* (4), 2815−2823.
(23) Gang, O.; Zhang, Y. *ACS Nano* **2011**, *5* (11), 8459−8465.
(24) Nguyen, T. D.; Jankowski, E.; Glotzer, S. C. *ACS Nano* **2011**, *5* (11), 8892−8903.
(25) Zhang, Y.; Lu, F.; van der Lelie, D.; Gang, O. *Phys. Rev. Lett.* **2011**, *107* (13), 135701−135701.
(26) Damasceno, P. F.; Engel, M.; Glotzer, S. C. *ACS Nano* **2012**, *6* (1), 609−614.
(27) John, B. S.; Stroock, A.; Escobedo, F. A. *J. Chem. Phys.* **2004**, *120* (19), 9383.
(28) Chan, H.; Demortière, A.; Vukovic, L.; Král, P.; Petit, C. *ACS Nano* **2012**, *6*, 4203−4213.
(29) Sun, Y.; Xia, Y. *Science* **2002**, *298* (5601), 2176−2179.
(30) Zeng, H.; Rice, P. M.; Wang, S. X.; Sun, S. *J. Am. Chem. Soc.* **2004**, *126* (37), 11458−11459.
(31) Bigioni, T. P.; Lin, X.-M.; Nguyen, T. T.; Corwin, E. I.; Witten, T. A.; Jaeger, H. M. *Nat. Mater.* **2006**, *5* (4), 265−270.
(32) Korgel, B.; Fitzmaurice, D. *Phys. Rev. Lett.* **1998**, *80* (16), 3531−3534.
(33) Hanrath, T.; Choi, J. J.; Smilgies, D.-M. *ACS Nano* **2009**, *3* (10), 2975−2988.
(34) Murray, C.; Kagan, C.; Bawendi, M. *Annu. Rev. Mater. Sci.* **2000**, *30*, 545−610.
(35) Wise, F. W. *Acc. Chem. Res.* **2000**, *33* (11), 773−780.
(36) Lu, W.; Fang, J.; Ding, Y.; Wang, Z. L. *J. Phys. Chem. B* **2005**, *109* (41), 19219−19222.
(37) Baumgardner, W. J.; Quan, Z.; Fang, J.; Hanrath, T. *Nanoscale* **2012**, *4*, 3625−3628.
(38) Choi, J. J.; Bealing, C. R.; Bian, K.; Hughes, K. J.; Zhang, W.; Smilgies, D.-M.; Hennig, R. G.; Engstrom, J. R.; Hanrath, T. *J. Am. Chem. Soc.* **2011**, *133* (9), 3131−3138.
(39) Dunphy, D.; Fan, H.; Li, X.; Wang, J.; Brinker, C. J. *Langmuir* **2008**, *24* (19), 10575−10578.
(40) Disch, S.; Wetterskog, E.; Hermann, R. l. P.; Salazar-Alvarez, G.; Busch, P.; Brückel, T.; Bergström, L.; Kamali, S. *Nano Lett.* **2011**, *11* (4), 1651−1656.
(41) Eggiman, B. W.; Tate, M. P.; Hillhouse, H. W. *Chem. Mater.* **2006**, *18* (3), 723−730.
(42) Kikegawa, T.; Iwasaki, H. *J. Phys. Soc. Jpn.* **1987**, *56*, 3417−3420.
(43) Crossland, E. J. W.; Kamperman, M.; Nedelcu, M.; Ducati, C.; Wiesner, U.; Smilgies, D. M.; Toombes, G. E. S.; Hillmyer, M. A.; Ludwigs, S.; Steiner, U.; Snaith, H. J. *Nano Lett.* **2008**, *9* (8), 2807−2812.
(44) Smith, D. K.; Goodfellow, B.; Smilgies, D.-M.; Korgel, B. A. *J. Am. Chem. Soc.* **2009**, *131* (9), 3281−3290.
(45) Heitsch, A. T.; Patel, R. N.; Goodfellow, B. W.; Smilgies, D.-M.; Korgel, B. A. *J. Phys. Chem. C* **2010**, *114* (34), 14427−14432.
(46) Hosemann, R.; Bagchi, S. N. *Acta Crystallogr.* **1952**, *5* (5), 612−614.
(47) Dullens, R. P. A.; Petukhov, A. V. *Europhys. Lett. (EPL)* **2007**, *77* (5), 58003.
(48) Berg, J. C., *An introduction to interfaces and colloids*. World Scientific: NJ, 2010.
(49) Kutuzov, S.; He, J.; Tangirala, R.; Emrick, T.; Russell, T. P.; Böker, A. *Phys. Chem. Chem. Phys.* **2007**, *9* (48), 6351−6351.
(50) Wi, H. S.; Cingarapu, S.; Klabunde, K. J.; Law, B. M. *Langmuir* **2011**, *27* (16), 9979−9984.
(51) Campolongo, M. J.; Tan, S. J.; Smilgies, D.-M.; Zhao, M.; Chen, Y.; Xhangolli, I.; Cheng, W.; Luo, D. *ACS Nano* **2011**, *5* (10), 7978−7985.
(52) van Rijssel, J.; Erne, B. H.; Meeldijk, J. D.; Casavola, M.; Vanmaekelbergh, D.; Meijerink, A.; Philipse, A. P. *Phys. Chem. Chem. Phys.* **2011**, *13* (28), 12770.